Supporting Information

Bifunctional LaF_3 Doping Strategy Achieving Coupled Bulk and Interfacial Reconstruction for Ni-rich Cathodes

Sihan Li,[#a] Yunhai Zhang,[#a] Le Zhao,[a] Huimin Ji,[a] Zhouhao Fu,[a] Jie Tan,[a] Jun Bao,[b] Yixin Li,[c] Qi Zhang,[a,*] Yougen Tang,[a] and Haiyan Wang[a]

[a] Hunan Provincial Key Laboratory of Chemical Power Sources, College of Chemistry and Chemical Engineering, Central South University, Changsha, 410083, P.R. China

[b] National Synchrotron Radiation Laboratory, IRFEL Innovation Center for Energy Chemistry, University of Science and Technology of China, Hefei, Anhui 230026, P.R. China

[c] Key Laboratory of Advanced Energy Materials Chemistry (Ministry of Education), Nankai University, Tianjin 300071, China

E-mail addresses: qzhang1027@csu.edu.cn (Q. Zhang).

1. Experimental Section

1.1. Materials Synthesis

The LaF_3 doped $LiNi_{0.9}Co_{0.05}Mn_{0.05}O_2$ (NCM90) were prepared by co-calcining LaF with NCM90. Specifically, the commercial-grade NCM90 (provided by Shenzhen Huaqing New Material Technology Co., Ltd..) and LaF_3 powder (AR, Macklin) were homogeneously mixed by ball milling (300 rpm/min, 3 h) then the obtained mixture was calcinated at 580 °C for 5 h in a heating/freezing rate of 1.5 °C/min under pure O_2. The molar ratios of NCM90 to LaF_3 were set at 1:0.05, 1:0.1 and 1:0.2, respectively, and the samples obtained were named NCM-0.05LaF_3, NCM-0.1LaF_3 and NCM-0.2LaF_3, respectively.

1.2. Characterization.

The crystallinity of the cathode was characterized by the powder X-ray diffraction (Bruker D8 advance) over a 2θ range of 5° to 80° with 2° min^{-1} and with Cu Kα radiation (λ = 1.5406 Å). The morphology of the sample was analyzed by SEM (TESCAN MIRA LMS). The micromorphology of the sample was characterized on a TEM and HR-TEM (FEI Tecnai F20). The specimens were prepared by focused ion beam scanning electron microscopy (FIB-SEM, FEI scios, 20 kV). The surface elemental composition of the sample before and after cycling was investigated by an X-ray photoelectron spectrometer (XPS, Thermo Scientific K-Alpha). The etch voltage used for the X-ray photoelectron spectrometer depth profiling was 3 keV and the sampling time point was 0s, 60s, 120, 240s, 420s and 600s. The X-ray absorption fine structure (XAFS) spectra of Ni K-edge of samples were collected in transmission mode on Table XAFS-500A (Specreation Instruments Co., Ltd.) at 25 kV and 20 mA. The Si (551) spherically bent crystal analyzers with a radius of curvature of 500 mm were used. Before test, the samples were grinded and tableted into slices with diameter of 12.7 mm.

1.3. Electrochemical Measurements

The electrochemical properties of the prepared samples were tested using the NEWARE test system (CT-4008T-5V50Ma-164, Shenzhen, China) at 30 °C with a current density of 200 mA g^{-1} (1C) between of 3.0 and 4.3 V. The cathode material were mixed with super P and PVDF binder (mass ratio of 8:1:1) in N-methylpyrrolidone (NMP) solvent, then casted on Al foil, and dried at 110 °C for 6 h in a vacuum oven. The obtained cathode electrodes with active material mass of approximately 3.0 mg cm^{-2} were assembled into coin-type half cells (2016, provided by Canrd Technology Co. Ltd) in an argon-filled glovebox with Li metal and 1 M $LiPF_6$ (EC/DEC, 1:1 in volume) as the counter electrode and the electrolyte, respectively. The cycle test began after five cycles of charge and discharge at 0.1 C. The Electrochemical impedance spectroscopy (EIS) and Cyclic voltammetry (CV) analysis were performed using CHI660e electrochemical workstation. The galvanostatic intermittent titration technique (GITT) measurement was carried out at 0.1 C between 3.0 and 4.3 V, with 10 min charging/discharging periods and 30 min rest periods.

1.4. Theoretical Calculations

Density Functional Theory (DFT) Simulation

In this study, first-principles calculations were conducted using the Vienna Ab-initio Simulation Package (VASP)[1], based on Density Functional Theory (DFT)[2] and the Projector Augmented-Wave (PAW)[3] method. The Generalized Gradient Approximation (GGA) method with Perdew-Burke-Ernzerhof (PBE) pseudopotentials was employed to describe exchange-correlation interactions[4]. For the 3d orbitals of Ni, the Hubbard correction parameter Ueff (Ueff = U - J) was set to 6.2 eV[5]. To accurately describe the electronic wave functions, we selected a plane-wave kinetic energy cutoff of 520 eV and utilized a 3 × 3 × 1 grid for the gamma-centered Monkhorst-Pack K-point mesh[6]. The atomic positions were thoroughly relaxed until convergence criteria were met, with the maximum energy difference converging to 10^{-5} eV and the Hellmann-Feynman force on atoms reducing to 0.01 eV/Å[7]. The Density of States (DOS) analysis included both spin-up and spin-down states. Additionally, the Crystal Orbital Hamilton Population (COHP) was calculated using the LOBSTER program

2. Results and Discussion

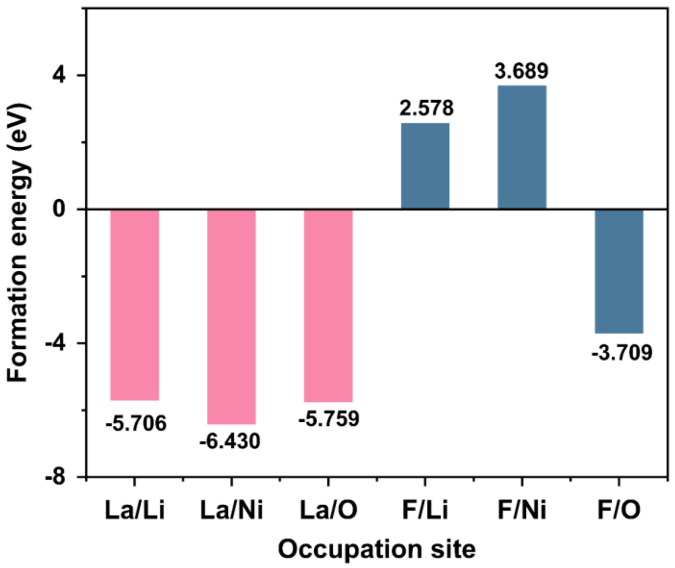

Fig. S1. The formation energies of representative occupancy sites for La/F atoms.

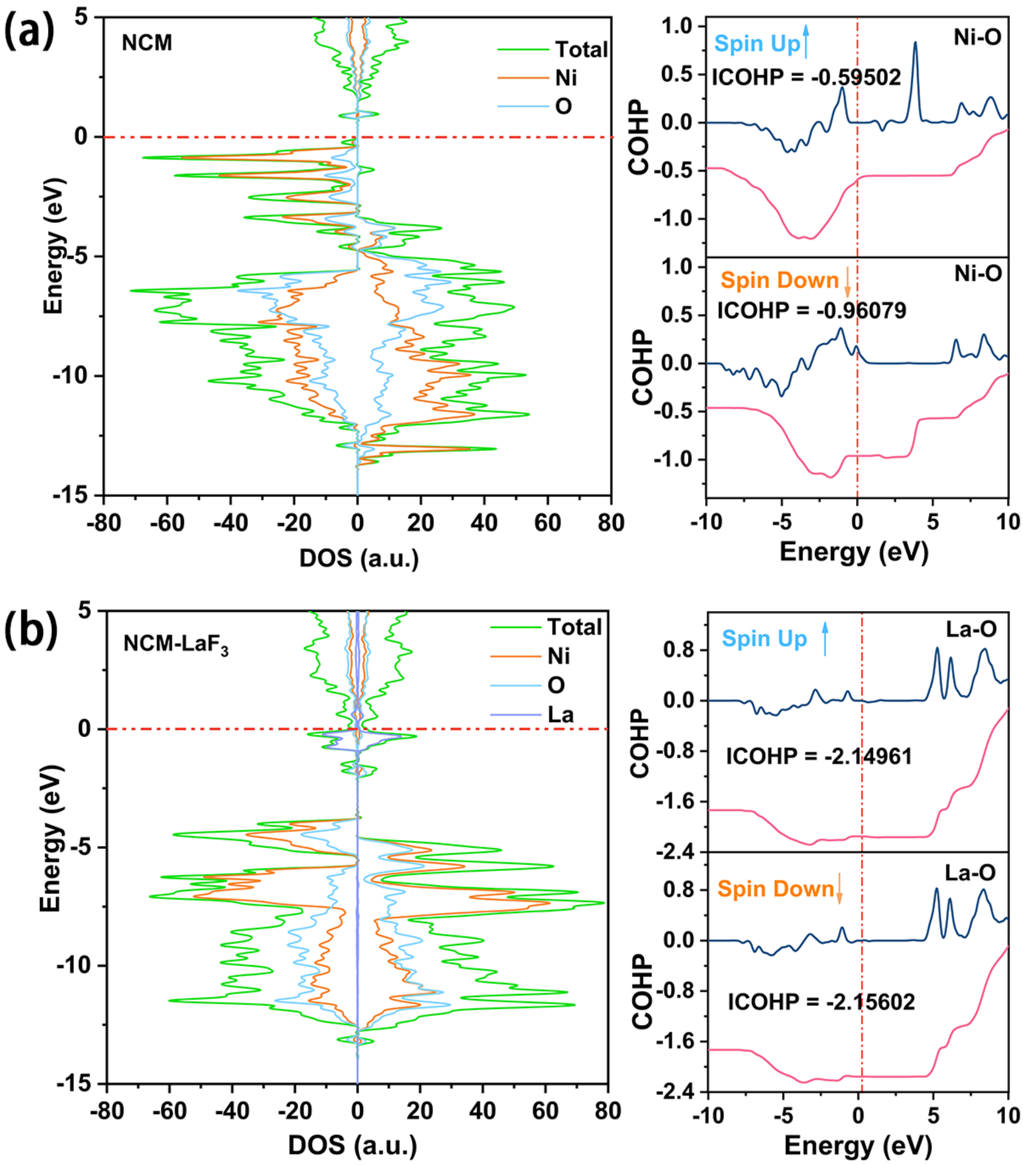

Fig. S2. DOS and COHP diagrams for a) NCM and b) NCM-LaF$_3$.

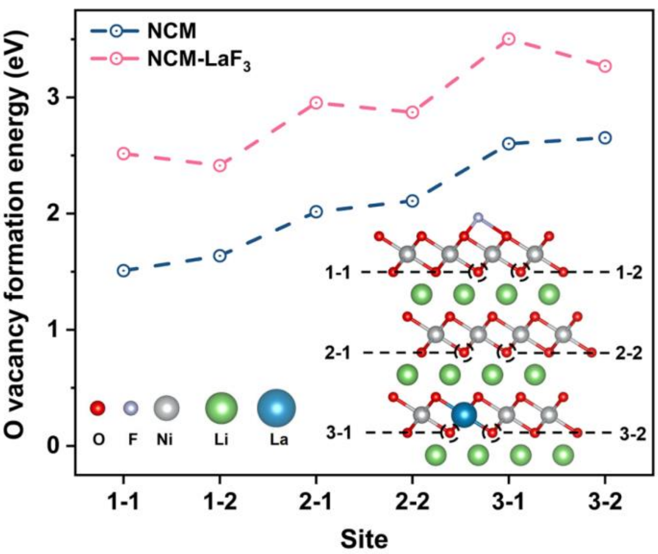

Fig. S3. Oxygen vacancy formation energy at different O site after LaF_3 doping.

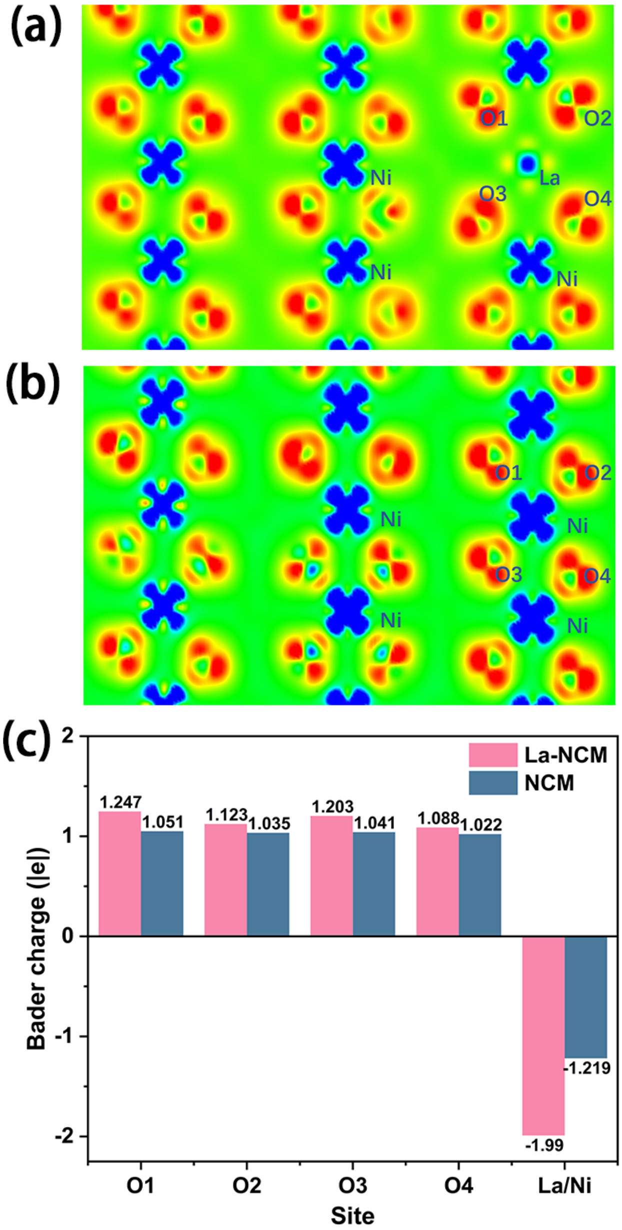

Fig. S4 The differential charge density of a) NCM-LaF_3 and b) NCM. c) The bader charge of different oxygen and metal sites (La or Ni) for NCM and NCM-LaF_3.

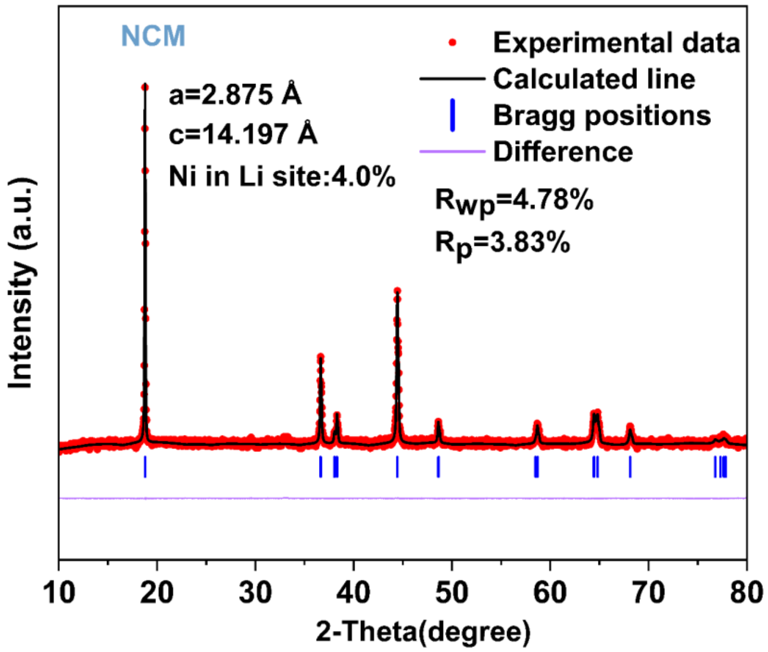

Fig. S5. Rietveld refinement of XRD for pristine NCM.

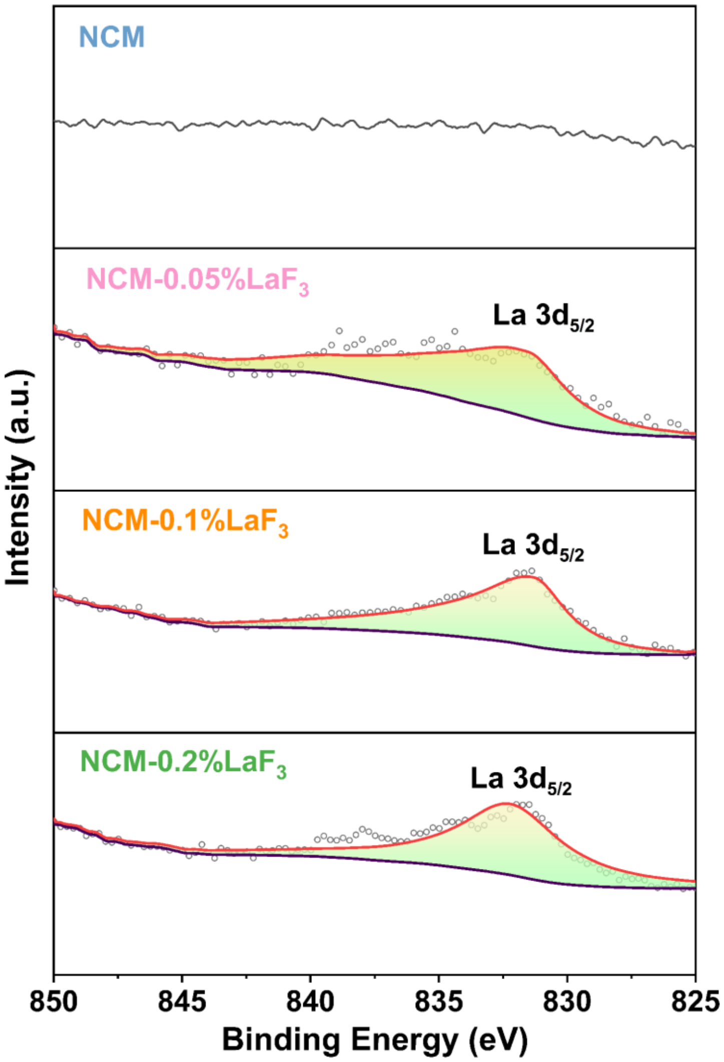

Fig. S6. XPS spectra of La 3d for for all samples.

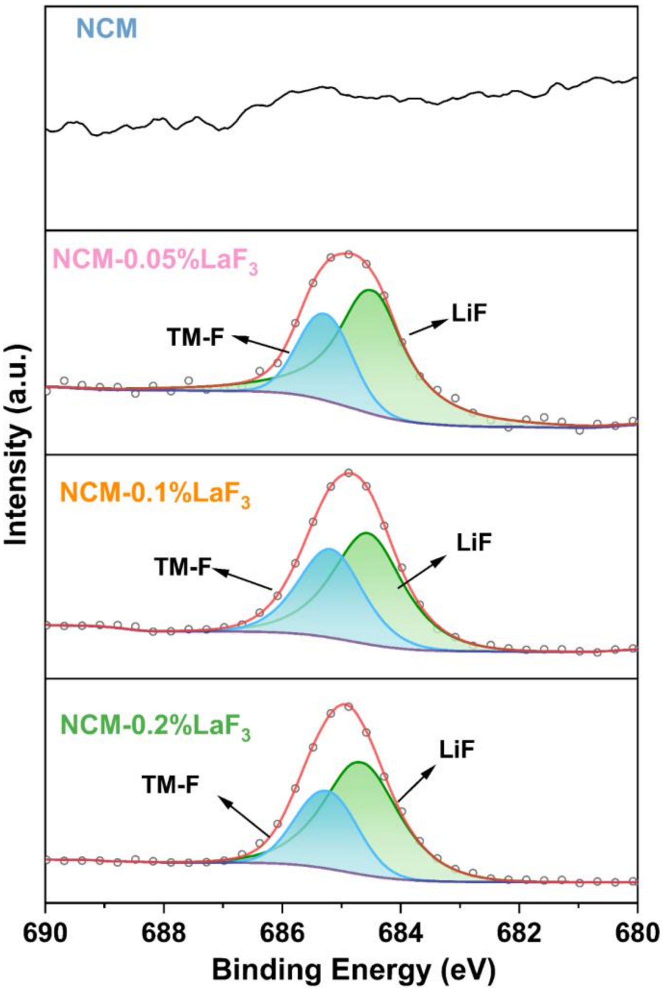

Fig. S7. XPS spectra of F 1s for for all samples.

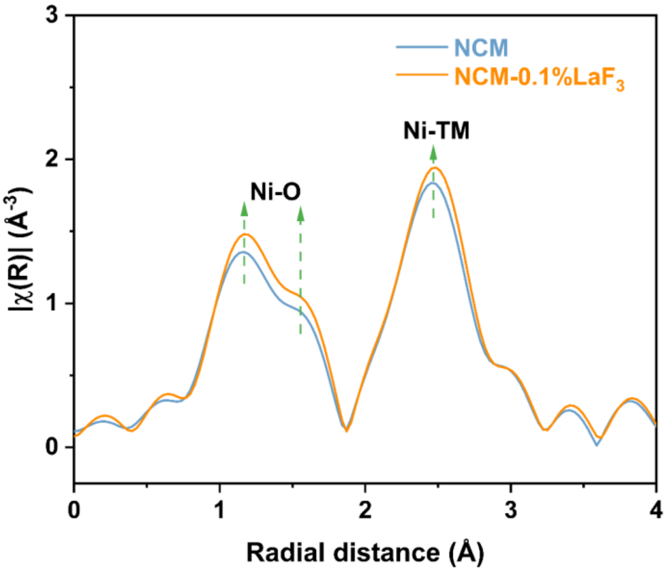

Fig. S8. EXAFS R space curves of Ni *K*-edge for NCM and NCM-0.1%LaF_3.

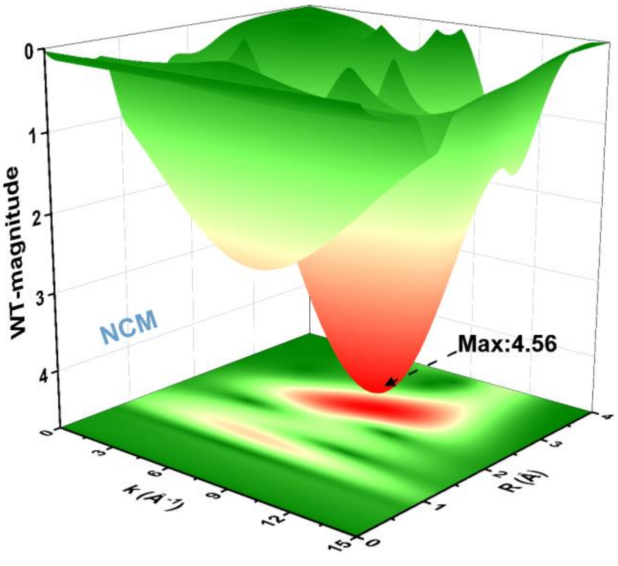

Fig. S9. EXAFS wavelet transforms images of Ni K-edge for pristine NCM.

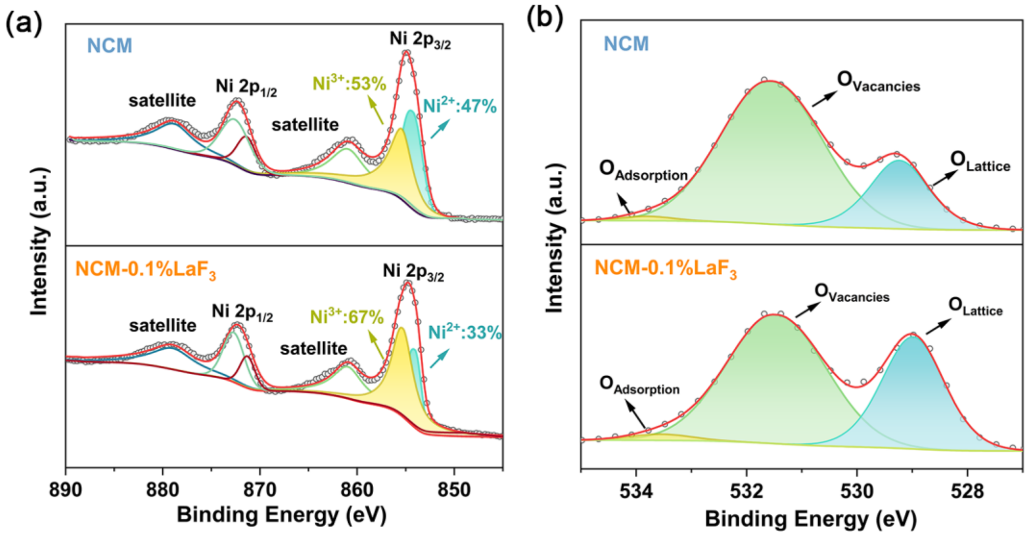

Fig. S10. XPS spectra of a) Ni 2p and b) O 1s for NCM and NCM-0.1%LaF$_3$.

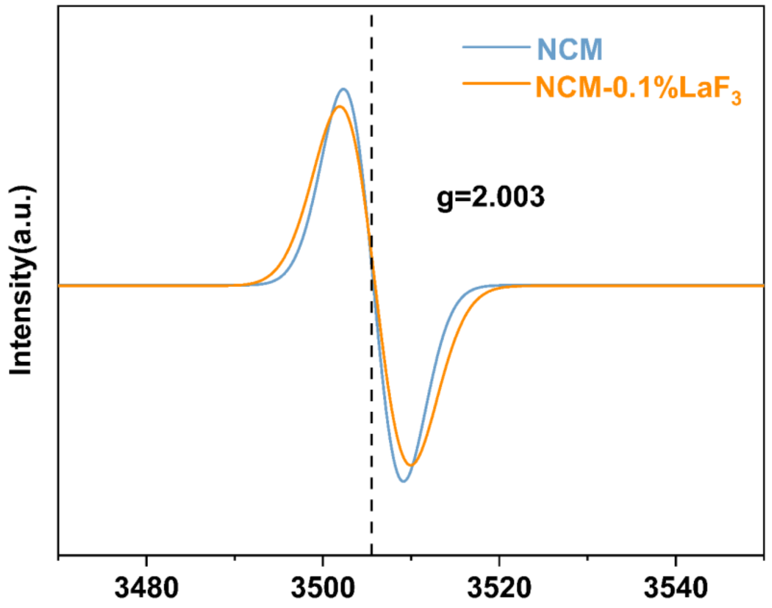

Fig. S11.EPR spectra of cathodes NCM and NCM-0.1%LaF_3.

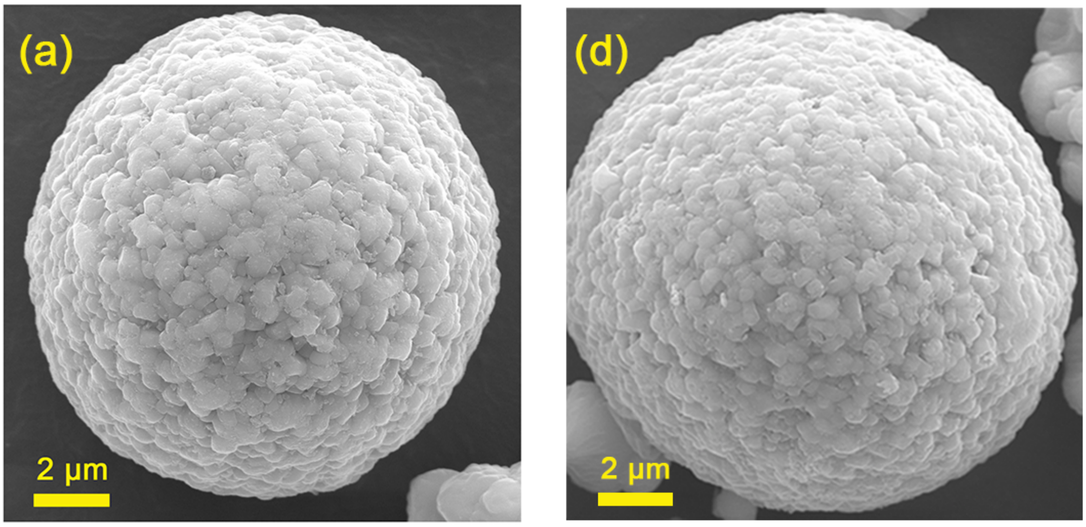

Fig. S12. SEM spectra for a) pristine NCM and b) NCM-0.1%LaF_3.

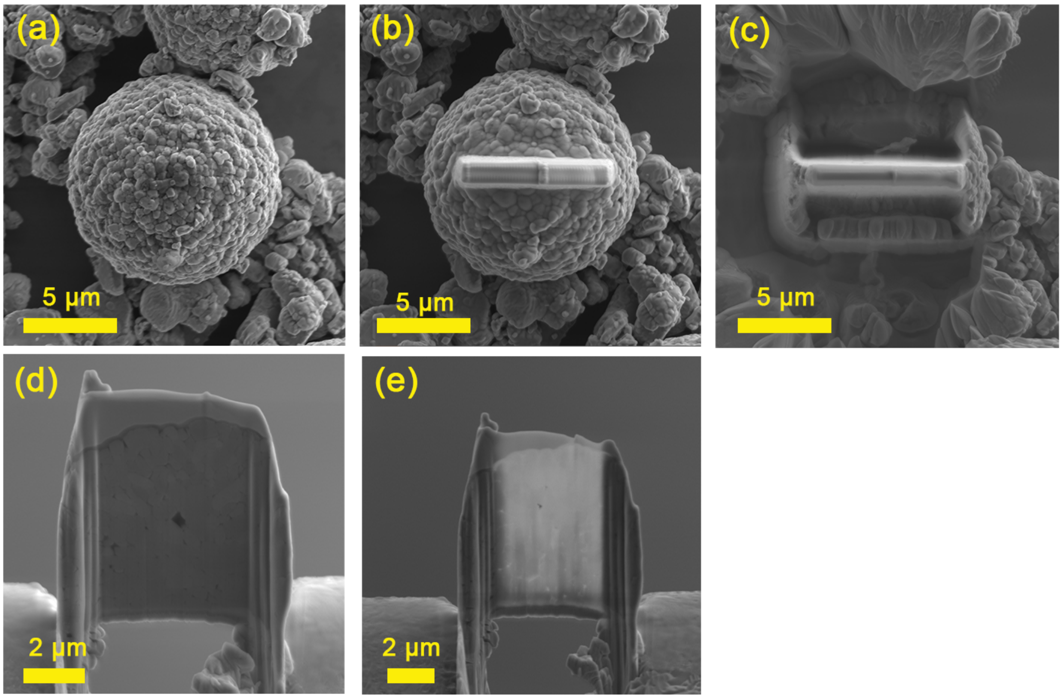

Fig. S13. SEM images of the preparation process of cross-section for NCM-0.1%LaF_3.

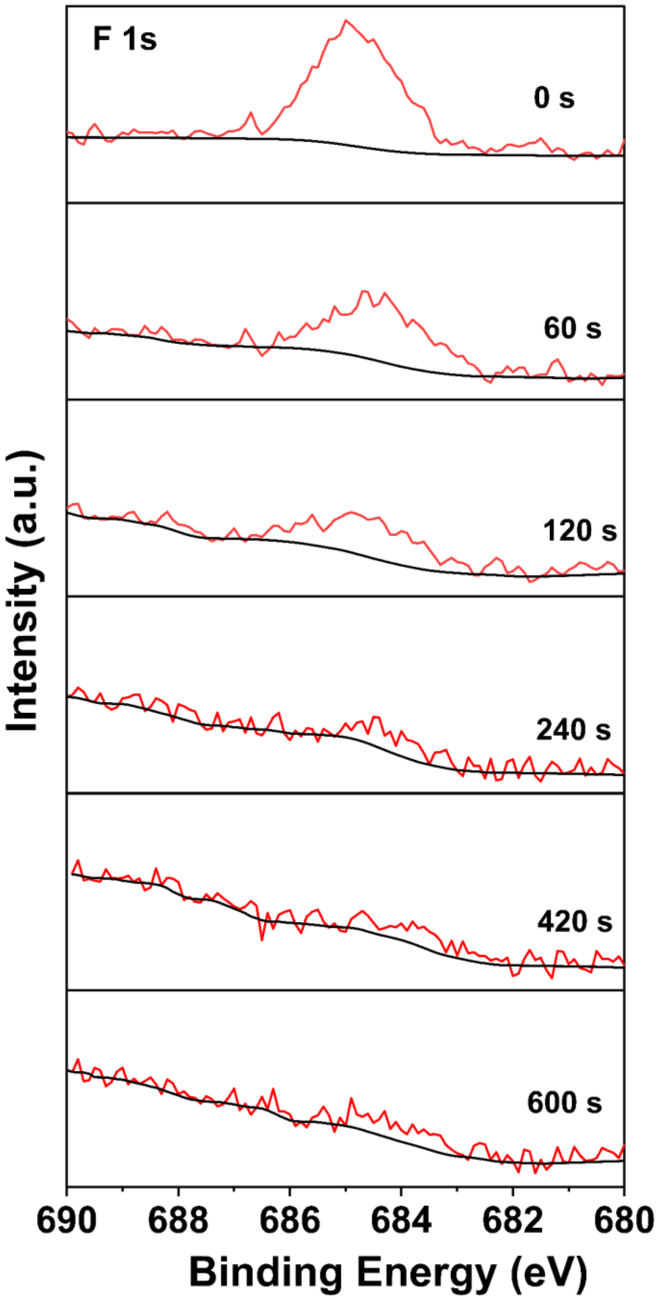

Fig. S14. XPS spectra of F 1s for NCM-0.1%LaF_3 at different etching times.

Note1#: The F content decreases as etching time increases (depth increases).

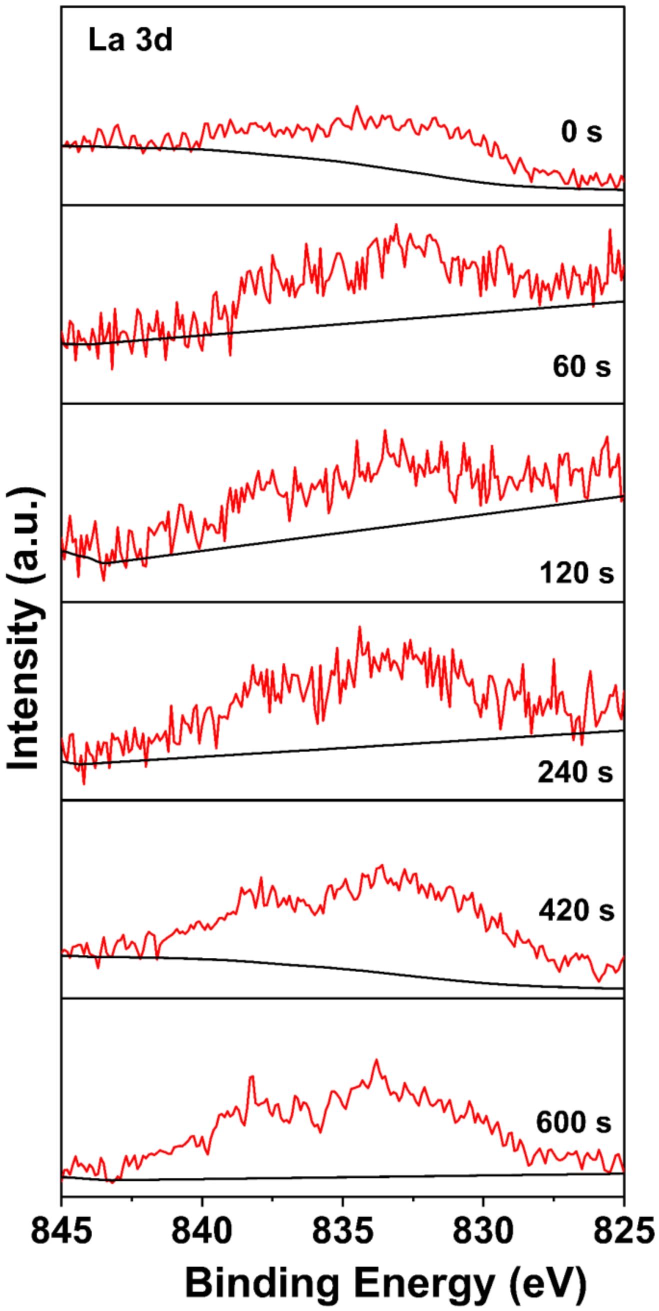

Fig. S15. XPS spectra of La 3d for NCM-0.1%LaF_3 at different etching times

Note2#: The La content gradually increases as etching time increases (depth increases).

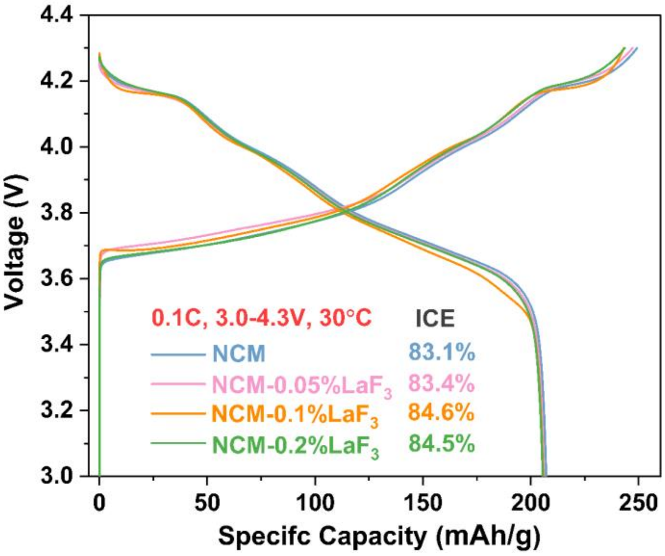

Fig. S16. Initial charge–discharge curves at 0.1C of as-prepared samples.

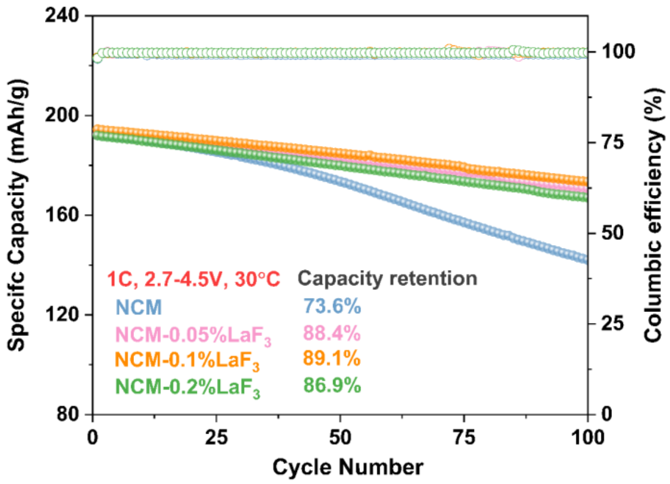

Fig. S17. Cycling performance at 1 C between 2.7 and 4.5 V of as-prepared samples.

Note3#: The pristine NCM material shows the most pronounced capacity decay, while all samples with doped LaF_3 doping exhibit improved cycling stability. These data indicate that LaF_3 doping is effective in improving the cycling stability of NCM cathode materials, with a concentration of 0.1% providing the best performance improvement.

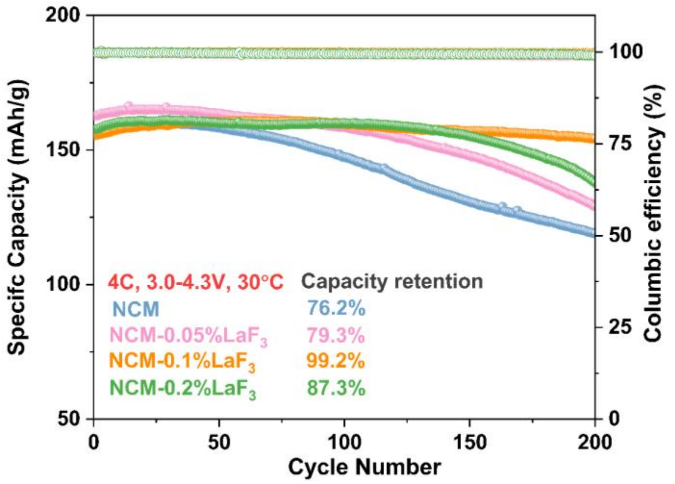

Fig. S18. Cycling performance at 4 C between 3.0 and 4.3 V of as-prepared samples.

Note4#: Under 4C rate, the 0.1% LaF_3-doped samples exhibit excellent cycling stability with close to 100% capacity retention, which is much better than the other samples. The NCM-0.1%LaF_3 with 87.3% retention, while the capacity retention of the NCM-0.05%LaF_3 was close to that of the original sample. Insufficient LaF_3 doping (0.05%) cannot effectively enhance the structural stability and Li-ion transport properties of the NCM material, resulting in rapid capacity decay at high C-rates. Conversely, excessive doping (0.2% LaF_3) may block the ion migration channels within the material or induce significant lattice distortions, leading to decreased capacity retention.

Note5#: By analyzing the electrochemical performance(Fig. 3, Fig. S16-18 ESI†), it can be concluded that NCM-0.1%LaF_3 has the optimal performance and the reason for this difference is related to the amount of LaF_3 doping. Specifically, the 0.05% doped samples showed limited improvement in bulk phase structural stability and surface interfacial protection due to the low content of La and F. The 0.2% doped samples negatively affected the lithium ion transport channels due to the increased lattice distortion caused by excessive La doping, while the excessive F may also form an excessively thick surface layer, increasing the charge transport impedance.The 0.1% doped samples achieved the optimal balance between bulk phase structural stability and the surface protection.

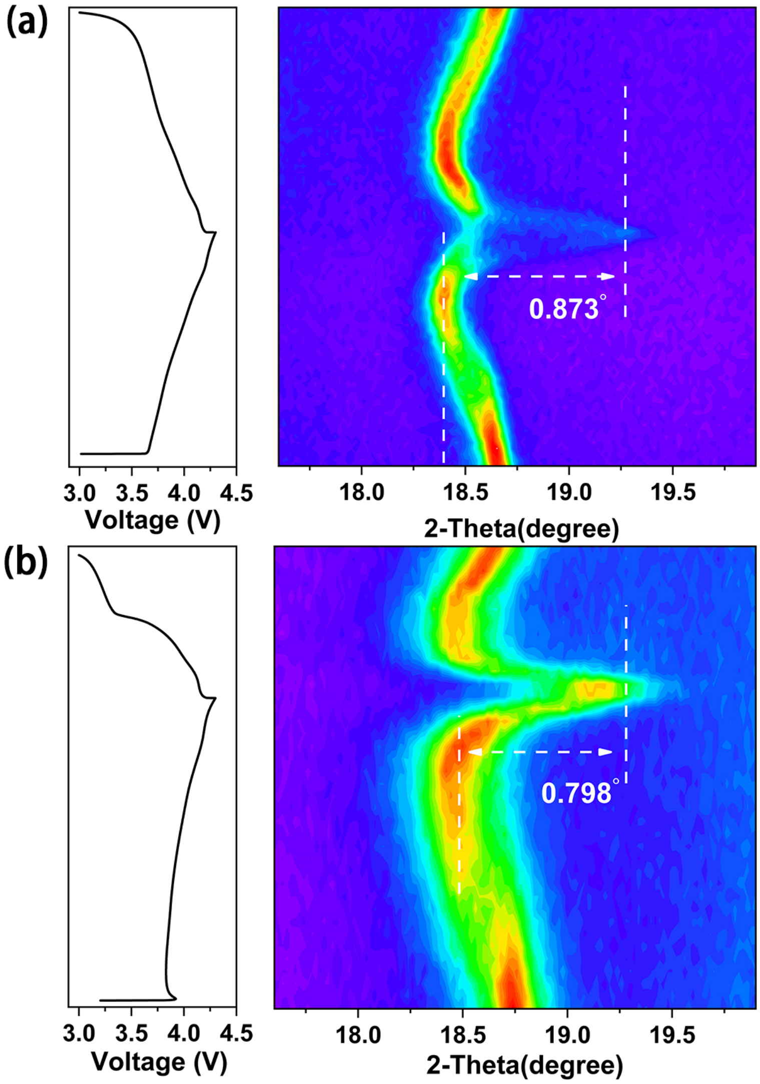

Fig. S19. Voltage profiles and contour map of the (003) diffraction patterns of the in situ XRD for a) pristine NCM and b) NCM-0.1%LaF_3.

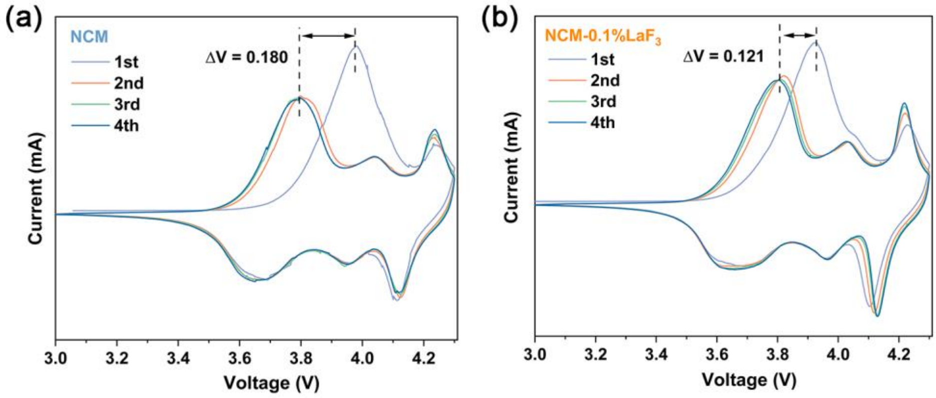

Fig. S20. CV spectra of a) NCM and b) NCM-0.1%LaF_3.

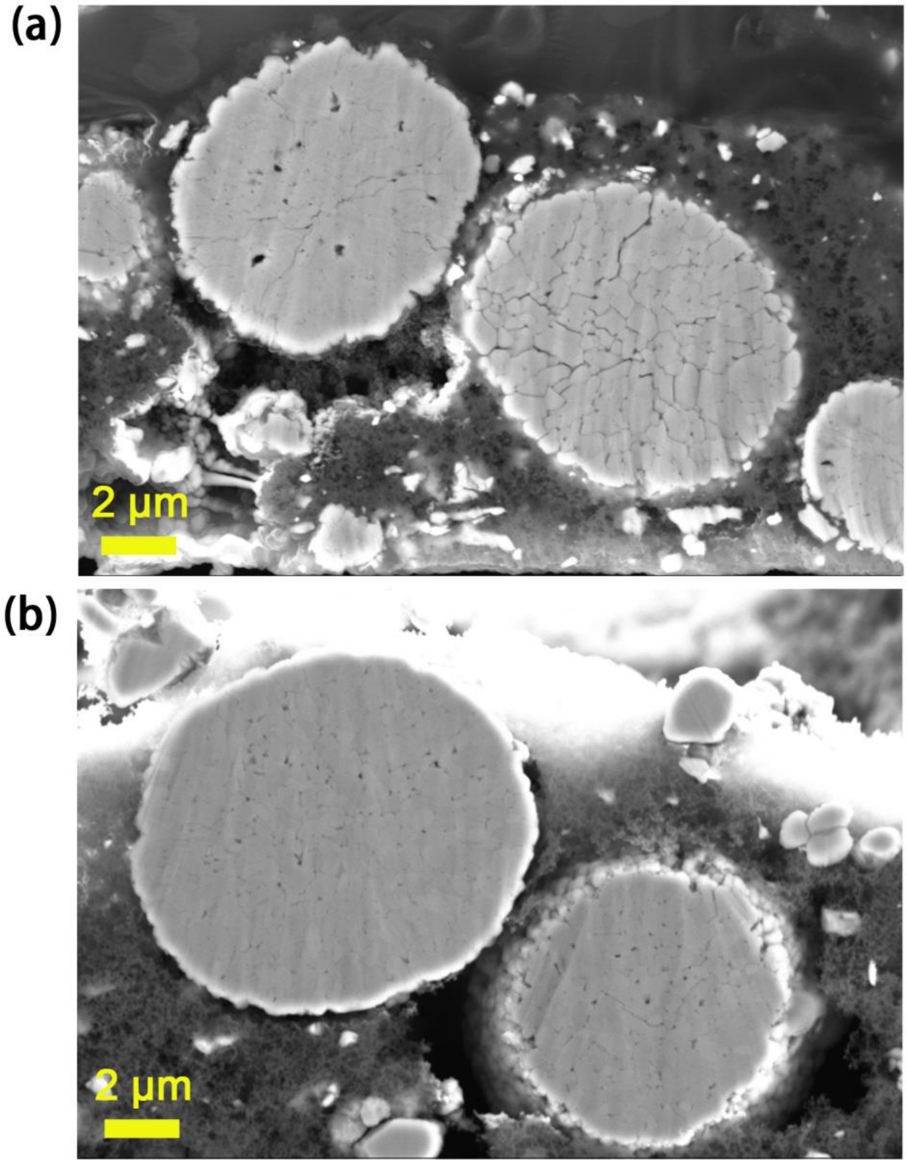

Fig. S21. Cross-sectional SEM images of a) pristine NCM and b) NCM-LaF_3 after 100 cycles at 1C.

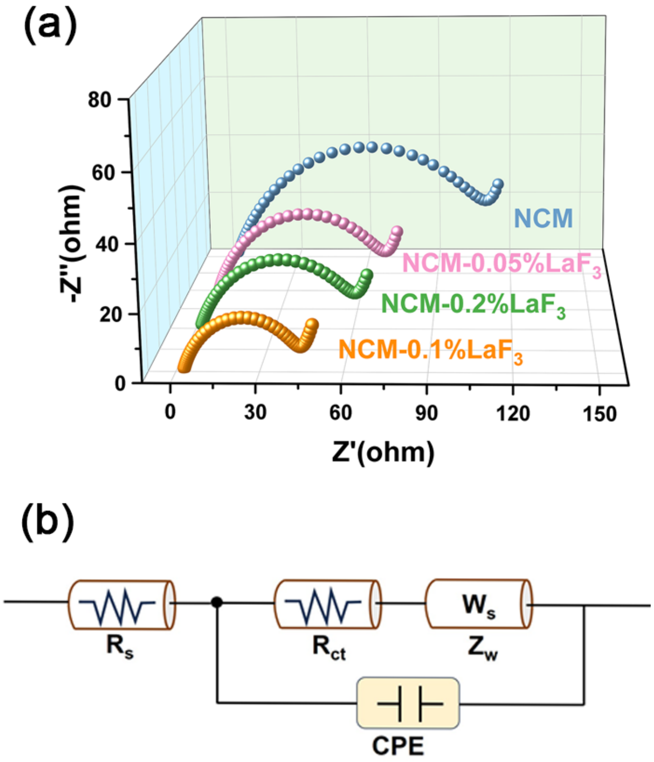

Fig. S22. a) EIS curves for the electrodes and b) equivalent electrical circuits of half-cell before the test.

Table S1 Corresponding parameters obtained from the Nyquist plots.

Samples	Before test		after 100 cycles at 1C		
	Rs	Rct	Rs	Rsf	Rct
NCM	3.1	112.6	6.4	54.6	641.1
NCM-0.05%LaF_3	2.1	68.8	3.9	30.7	166.5
NCM-0.1%LaF_3	2.7	43.3	6.5	16.7	92.6
NCM-0.2%LaF_3	1.69	59.5	2.2	53.4	153.8

Notes and references

1. G. Kresse and J. Furthmüller, *Physical Review B*, 1996, **54**, 11169-11186.
2. W. Kohn and L. J. Sham, *Physical Review*, 1965, **140**, A1133-A1138.
3. P. E. Blöchl, *Physical Review B*, 1994, **50**, 17953-17979.
4. J. P. Perdew, K. Burke and M. Ernzerhof, *Physical Review Letters*, 1996, **77**, 3865-3868.
5. H. Yang, H.-H. Wu, M. Ge, L. Li, Y. Yuan, Q. Yao, J. Chen, L. Xia, J. Zheng, Z. Chen, J. Duan, K. Kisslinger, X. C. Zeng, W.-K. Lee, Q. Zhang and J. Lu, *Advanced Functional Materials*, 2019, **29**, 1808825.
6. H. J. Monkhorst and J. D. Pack, *Physical Review B*, 1976, **13**, 5188-5192.
7. D. M. Ceperley and B. J. Alder, *Physical Review Letters*, 1980, **45**, 566-569.